ANNUAL REPORT

Portable Digital Mouth and Occlusion Reproducer

(KSTC-144-401-07-015)

PI: Fuhua (Frank) Cheng

Department of Computer Science
College of Engineering
University of Kentucky

Tel: (859) 268-5823
Email: cheng@cs.uky.edu
http://www.cs.engr.uky.edu/~ cheng/

4/25/2008

Summary

This is a summary of our work during the past ten months (June 1, 2007 - March 31, 2008). Technical tasks finished during this period include: the construction of a standard model, the construction of a occlusion model, the design of a mouth scan system, mesh simplification technique, mesh interpolation technique, mesh curvature computation technique, mesh segmentation technique, constraint based scaling, and offset surface generation technique. Technical tasks to be finished include: last step of the construction of the mouth scan system, and feature based matching technique. We expect our first prototype to be ready in three to four months.

We consider this grant, up to this point, a success. We not only have reached most of our research goals, i.e., developing the necessary imaging system and required geometric algorithms to support the reproduction of a patient's mouth and occlusion, but also produced an MS (Ds. Jiaxi Wang, graduated in March, 2008, currently working for a company in Lexington, KY), 3 journal papers and 2 conference paper. We anticipate another MS (Mr. Conglin Huang) to be produced at the end of this year and a PhD (Mr. Fengtao Fan) to be produced at the end of next year.

Table of Contents

1 Introduction

1.1 Background

Chairside CAD/CAM systems have been used by dentists for treatment of patients for more than 20 years. The first dental CAD/CAM system, CEREC 1 [123], was introduced to the dental community on Sept. 19, 1985 (see Figure 1(a) for such a system). The idea came out of one person: Dr. Werner H. Mörmann at the Dental School of the University of Zurich. Today, we have CEREC 3 (Figure 1(b)) and CEREC inLab [136]. Several other commercial

Figure 1: (left) CEREC-1; (right) CEREC-3.

dental CAD/CAM systems such as Cercon [84], Decim [75], etkon [88], Everest [106], GN-1 [97], DigiDent, DentaCAD [87], Lava [143], Medifacturing [68], Precident DCS [83], Procera [133], Pro 5O [80], Wol-Ceram [153], and ZENO Tec [151] are also available. All can do 3D design of veneers, inlays/onlays, crowns/Cores, bridges/frameworks [138]. The CEREC system, used by more than 17,000 dentists and in 28 dental schools in this country alone, remains the most popular one. It is possible now for a patient to go to a dentistry to get dental restoration service such as the ones mentioned above in only one trip [138]. However, one wouldn't be so lucky if a (removable) partial denture (Figure 2(a)) is needed. The patient will have to visit the dentistry at least three times and the total process will take more than 3-4 weeks. This is because the dentist still needs to take an *impression* of the patient's mouth (Figure 2(b)), send it to a dental lab for an experienced dental technician to make a partial denture (Figure 2(c)) out of it, wait for the partial denture to be sent back, try it on the patient, make necessary adjustment, and try on the patient again. More time will be needed

if the partial denture has to be sent back to the dental lab for structural modification.

(a) (b) (c)

Figure 2: (a) A partial denture, (b) a PVS-impression taken from a patient, and (c) making a partial denture.

One would ask: Current CAM technology should be able to handle the partial denture manufacturing process. So what is the problem here? Indeed, the required technology and materials are both there [96][123]. The problem is: we don't have a CAD representation of the patient's mouth required by a CAM system for the manufacturing process.

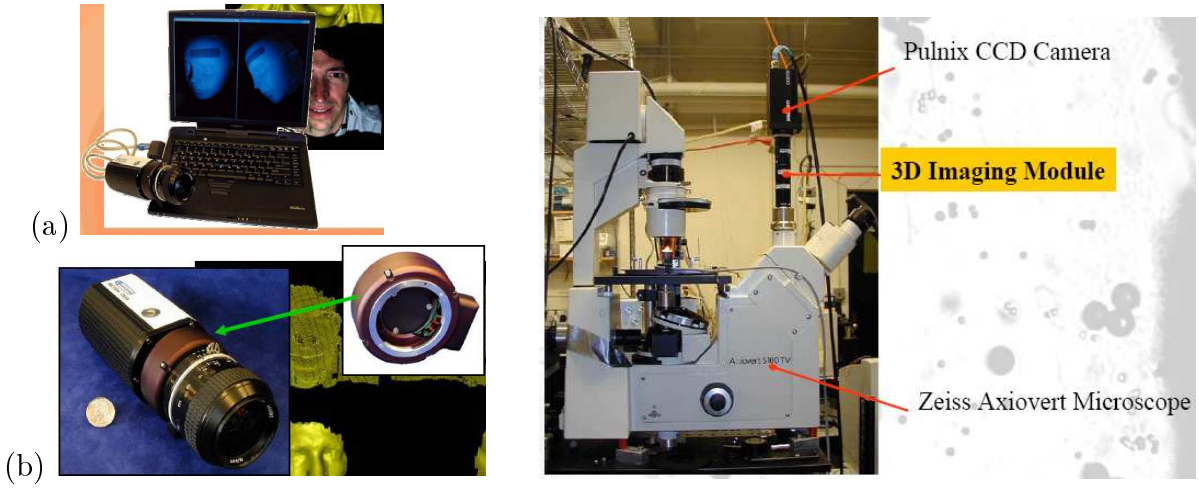

Figure 3: Brontes' product: (a) the 3D imaging system; (b) bolt-on camera; (c) system illustration.

1.2 Current Situation

[Intraoral Data Acquisition] Current intraoral data acquiring devices can be classified into three categories: *video camera based*, *X-ray based*, and *active wavefront sampling based*. In the first case, the hand-held device, mainly used as a visualization or inspection tool, can show live video of the teeth. The field of view is usually small, covering only one or two teeth (Figure 1). These cameras produce no 3D information that is critical for CAD/CAM design. Besides, for each tooth, they can only see part of it, not the entirety. Products in this category include Gendex's AcuCam series [95] and SUNI's SuniCam USB camera [140]. The Sirona's CEREC 3 camera [136] uses active infra-red light to acquire a depth map of the scene (Figure 1). A special painting is required and the reconstruction process takes about 45 seconds for just one tooth. It is difficult to extend it to build a 3D representation for the entire mouth. In the second case, by doing a full X-ray scan (200 X-rays or more), the device can get quite good 3D information of all the teeth and the jaws. Products such as Sirona's Galileos 3D [136], AFP Digital's Digital X-Ray [95], and Kodak's RVG Digital Radiographiy System [109] are in this category. But like all the X-ray images, this approach does not provide good information on soft tissues such as the gums which are critical in the reconstruction of the patient's mouth for partial denture design. In the third case, by using active projection to determine 3D surface data from 2D images [142][94], the single-camera device can actually see in 3D. Brontes' product is the only product in this category [74] (see Figure 3 for the imaging system, the camera and the system illustration of this product). However, like all the imaging systems, it can only provide information on visible portions of an object, it can not provide informtation on the portions of an object that it can not see. Therefore, with current intraoral data acquiring devices, it is not easy to acquire enough data for the construction of a complete CAD representation of a patient's mouth and the occlusion. That is why dentists are still using the impressing-taking approach to reproduce

a patient's mouth even though this approach has problems such as:

- the need of taking multiple impressions;
- remakes and multiple try-ins of the partial dentures due to poor quality of the impressions;
- over extended or under extended borders of the partial dentures; and
- dimension instability due to alginate shrinkage/expansion.

[**Shape Representation**] Another problem with the current chairside CAD/CAM systems is the *lack of design support for compact, one-piece representation of the mouth.* CAD representations supported by current chairside CAD/CAM systems are either *mesh based* or *NURBS-based* [145]. Mesh-based representations are expensive to maintain and process because usually excessively large amount of vertices and faces are needed in the representation to reach a required precision. On average, 20,000 vertices and faces are needed in a single tooth representation in this approach [145]. The NURBS-based approach, on the other hand, limited by the rectangular grid topology of its parameter space, can not represent complicated shape with only one surface. Therefore, current chairside CAD/CAM systems are hindered not only by insufficient data for the reconstruction of a mouth, but also inefficient CAD modeling techniques in representing the mouth.

2 Objective

The goal of this project is to develop a product called **Portable Digital Mouth and Occlusion Reproducer** (PDMOR) that is capable of reproducing the mouth and occlusion of a patient.

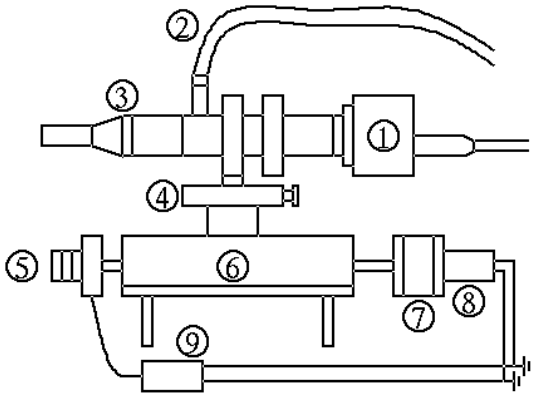

Figure 4: Conceptual deisgn of an MSS.

A PDMOR is composed of a *Mouth Scan System* (MSS), a flat-panel liquid crystal display (LCD) monitor, a PC, and a set of reconstruction, modeling and rendering programs (see Figure 4 for the design).

These components will be mounted on a small wheeled table to ensure easy mobility in a dental clinic or a dental lab. A dentist puts the MSS into the patient's mouth, instead of using the traditional *impression taking* approach, to get (multiple-view) image data of the visible portions of the teeth and gums of the patient. The image data then go through a triangulation, a feature detection and a registration processes to get an as complete as possible representation of the teeth and gums of the patient. This still incomplete representation is then combined with a standard model to reconstruct all the existing teeth and gums of the patient. The reconstructed 3D computer model can be used as a diagnostic aid for treatment planning or as a blue print for the design and manufacturing of dental appliances, such as partial dentures. It can also be used for patient education and identification purpose.

A PDMOR can reconstruct missing teeth of the patient according to appropriate parameters, and trim the mouth model in anyway a user desires. Therefore, this product will not only make the chair side job of a dentist easier, but also make the job of a dental technician in designing and manufacturing dental appliances, such as dental partials, easier and more

precise. Other advantages of this product include: no call-back is necessary for a patient, data can be sent to other places easier and data can be used for much longer time.

[**Technical Innovation**] The technical innovation of the project is two-fold: the *product* and the *technologies*. First, the development of PDMOR itself is revolutionary. No products have ever been developed (or, successfully developed) to reconstruct the complete mouth of a patient. This is the first time a product in that direction will be developed and marketed. The product will have significant impact on both dental practice and the dental industry. Actually, if a *centralized national dental database* can be built, this product will also have impact on dental record keeping, dental data transmission, remote treatment planning, and identification/security issue.

Second, the underneath idea of a PDMOR is also safe and innovative. With the camera being able to move axially, we have an imaging system that can see more points of the mouth than anybody else.

However, because of obstruction and constrained working space, no dental imaging systems can see all the points in the mouth of a patient, including ours. To use incomplete data to reconstruct the mouth, one needs to compare the acquired data of the patient with a standard model to determine how the standard model should be morphed and deformed to get a representation for each tooth and gum of the patient. This requires both novel modeling and novel representation technologies.

The reconstruction of a patient's occlusion is also necessary and important. A dental appliance, such as a partial denture, designed based on a mouth model without a proper occlusion pattern would not work because it can not perform chewing function properly (see Figure 5(b) for such a mouth model). Only a mouth model with an appropriate occlusion such as the one shown in Figure 5(a) can ensure proper function of the resulting partial denture.

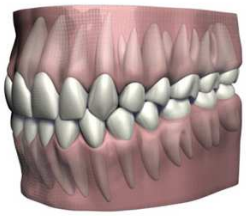

(a)

(b)

Figure 5: (a) Mouth with a working occlusion, (b) without a working occlusion.

3 Technical Tasks

Because the intraoral data acquiring process can not get complete data of the mouth, a standard model has to be used with the acquired data to build a patient's mouth and occlusion. The idea: for each tooth (gum) of the patient, we compare the acquired (partial) data of that tooth (gum) with the corresponding tooth (gum) in the standard model to determine how the representation of the standard model should be morphed and deformed to get a representation of that tooth (gum) for the patient.

This process involves several major technical steps. First, a standard model has to be built. This model should be able to provide information efficiently and accurately enough for all subsequent comparison, matching and morphing processes. Second, the data set received from the intraoral data acquiring process has to be segmented into groups so that the points of each group are either from an individual tooth or a gum.

For each resulting new data point group, we need to perform a *coarse-grained matching* [69] process to identify the corresponding tooth (gum) in the standard model. This process should be done using a *feature-based* approach to make it efficient. So we need to know the features of each segmented data group, as well as the features of each tooth and gum of the standard model [115]. We then perform a *fine-grained matching* to identify the exact location of each segmented data set on the representation of the standard model.

The next step is to *modify the standard model* so we can get a representation for each tooth and gum of the patient. This process involves rigid motions, scaling and deformation.

Everything up to this point is point-based. After this step, we need to perform a *surface fitting* process so a parametric representation can be obtained for each tooth and gum of the patient.

Techniqeus that have to be developed here include *feature detection*, *feature based matching*, *subdivision surface based interpolation techniques*, *point based data segmentation*, *point based 3D reconstruction*, *standard model construction*, *coarse-grained matching*, *fine-grained matching*, *morphing of subdivision surfaces*, *constraint based deformation*, *offset and blending subdivision surface generation*, and *subdivision surfaces intersection*. The standard model, the mouth model, and the occlusion of the patient will be represented by Catmull-Clark subdivision surfaces.

Subdivision surface based modeling and representation techniques are more powerful than NURBS or Splines based techniques in that

- the new techniques require only one surface to represent the final result no matter how complicated the shape and topology. This will not only make representation easier to handle, but make shape manipulation easier to perform as well;
- a voxel-based representation for the mouth model can also be created. This representation is good for visualization and virtual environment applications. But most importantly, it provides all the digital information required for subsequent design and manufacturing of the dental appliances and, hence, making the design and manufacturing process easier and more precise.

4 Experimental Method

In this section we explain how we realize our objectives.

[**Pointwise 3D Reconstruction**] Pointwise 3D reconstruction starts with the intraoral

data acquisition process, to be performed by the Mouth Scan System (MSS). An MSS is composed of an Axial Stereo Vision unit (see Figure 4 for the design of an Axial Stereo Vision unit). The concept of axial stereo vision has been studied for a while [130][81][139]. But usually only an oridnary lens is used in the system. Our design of the MSS is novel because it is the first time a cylindrical mirror is used in such a system. The parts of our Axial Stereo Vision unit are described as follows (see Figure 4(a) for the labels):

1. IEEE-1394 camera from Point Gray Research, the resolution is 1280×960
2. External light to camera, an xenon lamp cold light from LOEN Inc.
3. Cylindrical Mirror
4. Camera Mount
5. Position encoder from Microtech Laboratory Inc.
6. Translation stage
7. Gear box
8. DC motor. The motor will stop when the camera touches either end of the Translation Stage.
9. Motor power.

In our case, the cylindrical mirror could be very close to the target (teeth) when the system moves deeper into the mouth. In such a case, the *radial distortion* could be significant. On the other hand, the focal length of the mirror is relatively large in our system which helps reduce the significance of this error.

The solution for this distortion is to correct the image measurement to those that would have been obtained under an ideal pinhole lens. This process is illustrated in Figure 6 [139]. A thorough error analysis will be performed for this part.

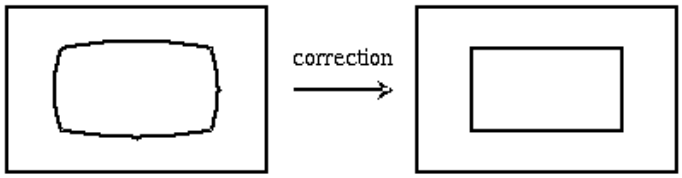

Figure 6: The image of a square with radial distortion and the corrected image.

In order to retrieve 3D coordinates from 2D images, the images need to be calibrated. The famous Tsai technique [146] will be used here. The remaining part of this task is well studied and developed in the literature.

[**Depth Reconstruction**] It is possible to calculate the depth information using an technique called *light attenuation sterro* (LAS). However, this new technique could fail if direct illumination is not strong enough to reach the back side of the teeth. With our novel approach of the MSS structure, we can use a technique called *multiview radial catadioptric imaging* to capture the teeth from just one shot [127].

[**Standard Model Construction**] since point based representation is too expensive for storage and processing, and information on individual teeth and gums is needed for the reconstruction process of teeth and gums of the patient, the best choice to build a standard model is to create a parametric representation for each individual tooth and gum. This will be done by scanning individual teeth and gums, forming a 2-manifold mesh with a desired combinatorial structure through triangulation of the unorganized point cloud, doing a simplification process to reduce the complexity of the 2-manifold mesh, and then performing a surface fitting process to get a parametric representation for each tooth and gum.

We don't anitcipate any technical problems for the first three steps. Actually the scanning process and the 2-manifold mesh generation process have already been done for all the

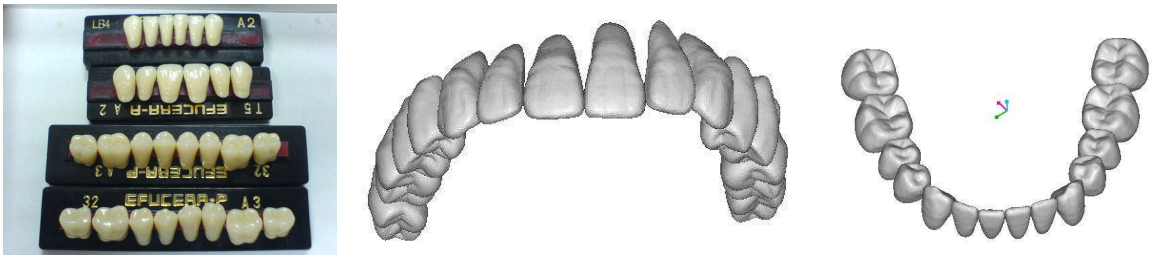

(a) (b) (c)

Figure 7: (a) Artificial ceramic teeth scanned for the standard model; (b) upper jaw teeth of the standard model; (c) lower jaw teeth of the standard model.

teeth (Figure 7). The third step, mesh simplification, is necessary because the number of points generated by the scanning process is very large (more than 20,000 points/faces generated for each tooth), way beyond the capability of any of the current surface interpolation technologies. A shape-preserving simplification technique [79] will be used for this step, although a technique published earlier can achieve the same goal as well [104]. The fourth step, however, requires special effort. Catmull-Clark subdivision surfaces (CCSSs) will be used for the fitting process [76]. We address the technical issues of this process next.

[Subdivision Surface based One-Surface Fitting] B-spline and NURBS surfaces have been used extensively in fitting 3D data points [90][91]. Because of the rectangular nature of their parameter spaces, they can only fit data points from a rectangular grid. They can not fit data points of arbitrary topology unless the data point set is segmented into groups each homeomorphic to a rectangular grid. But smoothness between the B-spline or NURBS surfaces that fit adjacent data point groups is not guaranteed. A better approach is to use subdivision surfaces in the fitting porcess because it is possible to fit any data points with only one subidivion surface and, consequently, no segmentation of the data set is required in the shape reconstruction process. Subdivision surfaces include uniform B-spline surfaces, piecewise Bézier surfaces, non-uniform B-spline surfaces and NURBS surfaces as special cases

[134]. So they are the most general surface representation scheme so far. See Figure 8(d) for the representation of a ventilation control component with a single subdivision surface. The initial control mesh and the control meshes after one refinement and two refinements are shown in (a), (b) and (c), respectively. The ventilation control component has seventeen holes (handles). Therefore, it can not be represented by a single B-spline or NURBS surface.

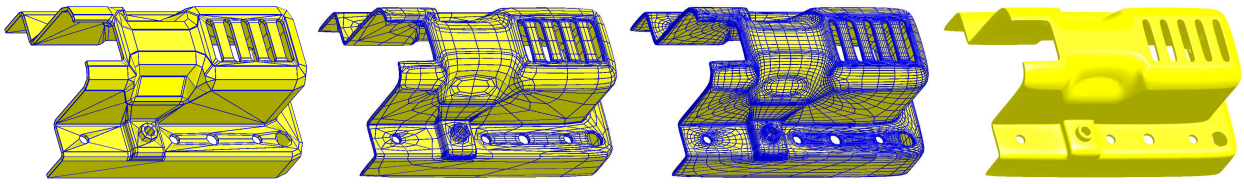

(a) (b) (c) (d)

Figure 8: (a) Initial control mesh, (b) control mesh after one refinement, (c) after two refinements, and (d) limit surface of a ventilation control component.

The fitting process will follow the following path. First, we perform one or more levels of Catmull-Clark subdivision on the given data points P to get a finer control mesh G. G satisfies the following property: each face of G is a quadrilateral and each face of G has at most one extra-ordinary vertex. The vertices of G are divided into two categories. A vertex of G is called a Type I vertex if it corresponds to a vertex of P. Otherwise it is called a Type II vertex. Q is then defined as a control mesh with the same number of vertices and the same topolgy as G. We assume Q has m vertices $Q = \{\mathbf{Q}_1, \mathbf{Q}_2, \cdots, \mathbf{Q}_m\}$, $m > n$, and the first n vertices correspond to the n Type I vertices of G (and, consequently, the n vertices of P). These n vertices of Q will also be called Type I vertices and the remaining $m - n$ vertices Type II vertices. This way of setting up Q is to ensure the parametric form developed for a CCSS patch [20] can be used for the limit surface of Q, denoted $\mathbf{S}(Q)$, and we have enough degree of freedom in our subsequent work. Note that m is usually much bigger than n. The remaining job then is to determine the position of each vertex of Q. The difference from previous work here is we will ignore the similarity constraint, focus on the

properties of the surface itself only. Figure 9 is an example from our work in this direction [?].

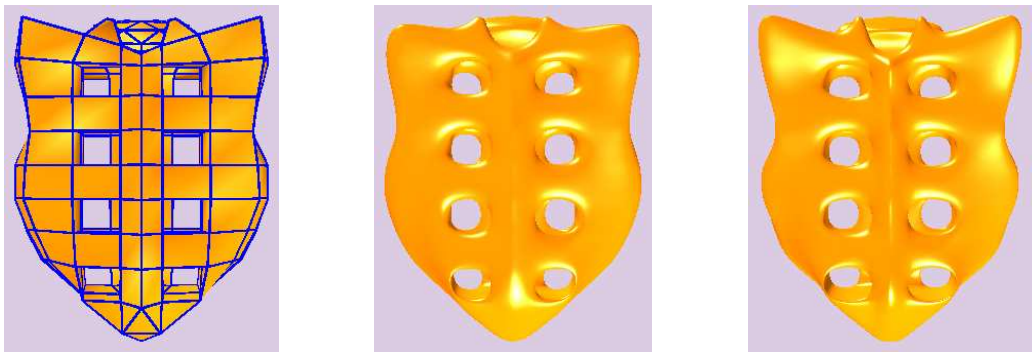

(a) (b) (c)

Figure 9: (a) Given data mesh M, (b) limit surface of M, (c) subdivision surface intgerpolates M.

[**Point based Data Segmentation**] In this research, segmentation of 3D points sampled by the intraoral data acquisition device will be done using a combination of edge-based approach [115] and region-based approach [148]. First, this is possible because topological information on the data sets is known, therefore seed surfaces can be defined for a region-based approach. Second, this is necessary because the 3D data set received from the data acquisition process does not contain many of the natural boundaries between adjacent teeth (the camera can not see them), therefore an edge-based approach can not do the work completely by itself. An edge detector designed as a convolution mask will be created first. The edge detector combines the functions of Gaussian smoothing and differential property estimation. Edge detection is then a zero crossing search in the convoluted signal [77]. The information received from the edge detector will be combined with all the boundaries of the gaps in the data set to form the path in doing the segmentation.

[**Coarse-Grained Matching**] A natural attempt here is to use the outline of each segmented data group to compare with the outlines of the teeth and gums in the standard

model to determine the correspondence. This naive approach works for the front teeth, maybe even the canine teeth, but not the other teeth because in most of the cases the camera can not see the entire tooth, therefore, the outline of the segmented data group does not represent the real outline of a tooth. Geometric features of the segmented data group will have to be used as well.

For each segmented data group, we will identify geometric features using a point-based approach [115], focusing on *corners* and *ridges*. For teeth and gums in the standard model, the features will be identified by examining the curvature of the subdivision surface representation. Note that parametrization techniques for Catmull-Clark subdivision surfaces are available [20][159][51]. Therefore, identifying features for objects represented by Catmull-Clark subdivision surfaces is possible.

[**Fine-Grained Matching**] The job here is, for each tooth and gum of the standard model, find its best position respect to the segmented, partial representation of the corresponding tooth (if there is one) or gum of the patient. This conceptually simple task is the most critical step of this research because the correctness of the reconstruction result and, consequently, the fitness of the partial denture(s) to be designed subsequently are largely determined by the result of this step. This step starts with the positioning of the gums, and then the front teeth, the molar teeth and the remaining teeth (in that order). The matching will be done by minimizing the distances between critical points of the corresponding teeth and gums with the location of the teeth with respect to the gums as constraints.

The distance will be defined by a local quadratic approximation to the *squared distance function* (SDF) [132]. Given a surface S, the SDF assigns every point P of the embedding space the squared distance from P to S. SDF has been applied to solve a number of shape fitting problems [131][78][149]. The local properties of the SDF for a manifold are presented in [63]. Its geometry is studied in detail in [132]. The advantages of SDF include (1) one can

completely avoids the parametrization problem, (2) the approximation procedure is faster and more stable. Our approximation is defined as follows.

Let S be an oriented surface $S(u, v)$ with a unit normal vector field $n(u, v) = e_3(u, v)$. At each point $S(u_0, v_0)$, we define a local right-handed frame whose first two vectors e_1 and e_2 determine by the principal curvature directions. These vectors are not uniquely determined at an umbilical point, but in that case we can take any two orthogonal tangent vectors e_1 and e_2. The defined frame is referred as the principal frame M. The two principal curvature centers at the considered surface point $S(u, v)$ can be expressed in M as $(0, 0, p_i)$. The quadratic approximant F_d of d^2 at $(0, 0, d)$ is given by:

$$F_d(x_1, x_2, x_3) \;=\; (d/(d-p_1))x_1^2 \;+\; (d/(d-p_2))x_2^2 + x_3^2$$

[Morphing of Standard Model] In general, due to change of curvature distribution after a scaling process, it is not possible for the new surface $\bar{\mathbf{S}}$ to have exactly the same shape and dimension as the unconstrainedly scaled surface while carrying all the original features. An approximation method has to be used to construct $\bar{\mathbf{S}}$. In this work, the new surface will be constructed following the *fix-and-stretch* based approach [55].

The main idea of this approach is to fix regions of the given subdivision surface that contain the features while scaling and stretching the remaining part of the surface until some conditions are reached (see Figure 10). The surface is divided into three parts, the features (region I of the smaller ellipse in Figure 10), neighboring regions of the features (region II in Figure 10), and the remaining part (region III in Figure 10). The features that need to be fixed during the scaling and stretching process have to be transformed to appropriate locations first (see region I of Figure 10). Region III is simply scaled using the given scaling factors. Region II is stretched to provide a smooth connection between the

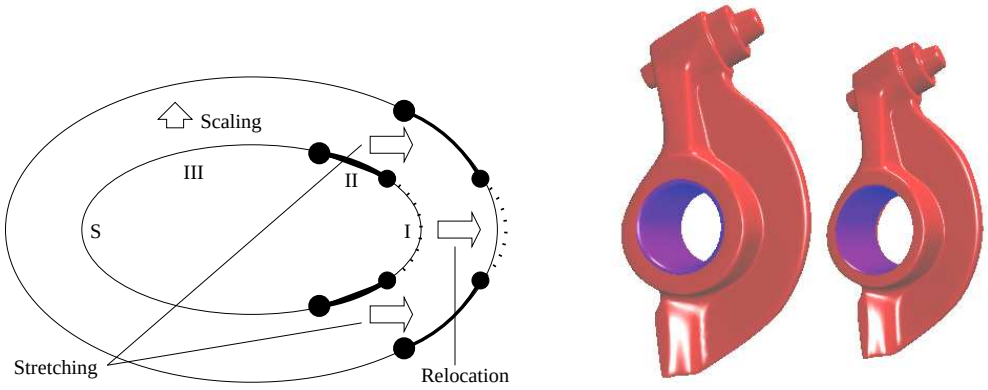

(a) (b)

Figure 10: (a) Basic idea of the fix-and-stretching approach, (b) constrained scaling: before (left) and after (right).

relocated features and the scaled region III.

The stretching process ensures that the shape and curvature distribution of $\bar{\mathbf{S}}$ are as close to those of the unconstrainedly scaled version of the given CCSS, $\hat{\mathbf{S}}$, as possible, while carrying all the original features $\mathbf{C}_i$. This is achieved by minimizing a shape-preserving objective function defined on the difference of these two surfaces on neighboring regions of the features. Efficient techniques have been developed for the energy evaluation process and the optimization process. The stretching process does not change the topological structure of the subdivision surface. Therefore, the resulting surface $\bar{\mathbf{S}}$ is again a CCSS. Figure 10(b) shows an example of this concept where the hole of the rocker arm is the feature held changed during the stretching process.

[Constraint Based Deformation] We need an automatic shape shrinking/expanding method for subdivision surfaces that would stop the shrinking/expanding process once some pre-set conditions are met. In this case, the pre-set conditions are locations of adjacent teeth, teeth on the opposite jaw, and information we received from the segmented results of the incomplete representation of the teeth and gums.

The difference between this technique and the technique presented in [55] is that in this

Figure 11: constraint based deformation: (a) before deformation; (b) after deformation.

case, the entire surface is scaled while, in the latter case, only certain portions of the surface are scaled (see Figure 10 for details). Another difference is, in this case, the scaling is not uniform even the entire surface is scaled (see Figure 11).

A yet third difference is, to ensure the partial denture is locked tight enough by its adjacent teeth, the above constraint should be slightly over-satisfied, i.e., the shrinking/expanding process does not stop immediately once the surface touches adjacent objects, but continues the shrinking/expanding process until an offset boundary condition is reached. One way to satisfy this condition is to scale down the size of the adjacent teeth slightly, and use the new shapes as the constraints. Another issue is, if the shrinking/expanding process touches one side first, one should modify the orientation of the subdivision surface instead of its location. The physical meaning of this is, the tooth should be sheared instead of moved.

[**Offset and Blending Subdivision Surface Generation**] For a given subdivision surface $\mathbf{S}$, the work we need to do here is to create an offset surface $\mathbf{S}^*$ for a specified portion of the given surface. Since subdivision surface is almost everywhere regular except at a few extraordinary points, an intuitive approach is to partition the specified region into sub-regions of rectangular topology and use the well-studied offset surface generation for conventional parametric surfaces (see, e.g., [67]) to generate an offset surface for each sub-region and then stitch these offset surfaces up to form an offset surface for the entire region. This seemingly reasonable approach gives us a surface that is smooth only in the interior of the partitioned

sub-regions, not at the boundary curves. This is not acceptable in our case because a partial denture manufactured using this model would have sharp edges at the sub-region boundaries and hurt the patient. Our approach here is to use a combination of constrained scaling and constrained translation to get a general offset surface generated and then use surface-surface intersection to remove undesired portion of the surface. This approach is independent of the topology of the base surface and, consequently, can be used for surfaces who parameters are not rectangular such as subdivision surfaces.

A blending surface will be generated by mixing several base surfaces to form a new surface. Each base surface contributes certain share in the formulation of the new surface. The weight of each base surface is determined by a real-valued function called "$weightfunction$" or "$blendingfunction$". Blending surface generation for B-spline and B'ezier surfaces has been well studied [73]. As in the offset surface generation case, those techniques can not be uses directly because the presence of extra-ordinary points.

The basic idea is to construct a rail curve on both surface, using the surface-surface intersection technique to be developed next, then build a general blending model. This is because the construction of a smoothing surface for two intersecting surfaces requires the computation of the intersection curve in certain cases only. The computed intersection curve does not have to be exact; a good approximation would usually be enough. After all, this curve is only used in generating two appropriate rail curves and an appropriate blending area. Note that the construction of the rail curve and the blending area should be performed in parameter space to avoid unnecessary adjustment process. Another important issue in this direction is the smoothing of sharp edges and sharp corners. A blending technique for the smoothing of a sharp corner shared by three faces will be developed here too.

[**Subdivision Surfaces Intersection**] The intersection operation will be performed in the parameter spaces of the subdivision surfaces, not in object space. A *cubic frame buffer* will be

created for each closed subdivision surface (a solid: a tooth or a gum). The representation of each tooth (gum) will be voxelized first and then a *volume flooding* is performed to mark all the voxels that are inside the given tooth (gum). Therefore, voxels in each cubic frame buffer can be classified into three categories: (1) *IN* voxels, (2) *ON* voxels and (3) *OUT* voxels. Let

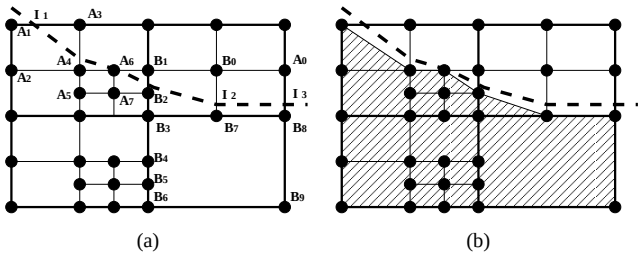

Figure 12: Performing intersection operation in 2D parameter space.

$\mathbf{S}(u, v)$ be a patch of the CCSS representation of a tooth (gum) A. For each subpatch of $\mathbf{S}(u, v)$ resulted from the voxelization process, we voxelize it one more time using the method discussed in [50]. However, this time we do not write voxels into A's cubic frame buffer, but look up the voxel values in both tooth A and tooth B's cubic frame buffers. If voxel values of this subpatch in both cubic frame buffers are either *IN* or *ON*, then this is a subpatch to keep. Subpatches of this type will be called *K-subpatches*. If voxel values of this subpatch are all *OUT* in both cubic frame buffers, then this is a subpatch to discard. Subpatches of this type are called *D-subpatches*. Otherwise, i.e., if some of the voxel values are *IN* or *ON* and some of the voxel values are *OUT*, then this is a patch with some portion to keep and some portion to discard. Subpatches of this type are called *I-subpatches* (intersecting subpatches). For example, the rectangles shown in Fig. 12 (a) are the parameter spaces of the resulting subpatches when the recursive voxelization process stops and the dashed polyline is part of the intersection curve of the two given teeth in this patch's 2D parameter space. We can see that subpatch $\mathbf{A}_1\mathbf{A}_2\mathbf{A}_4\mathbf{A}_3$ in Fig. 12(a) is an I-subpatch. The intersection curve detecting process then basically is process to trace the I-subpatches.

[**Outcome Assessment**] We will use only one metric in assessing the outcome of the innovation research described above. We will consider the outcome a good one if the *relative error* in each case is smaller than or equal to 3% of the dimemsion of a tooth. Measuring *absolute error* does not make much sense here because the dimension of a tooth is already relatively small. The reason for using 3% for the relative error bound is because it corresponds to half a pixel in a resolution of 1280×960. This bound will be used both for DMR and shape representation.

5 Results and Discussion

[**Mouth Scan System**] We have performed comparison of two different designs. In the first case, the camera looks through the cylindrical mirror (the axis of the mirror and the camera's optical axis are coincident). The camera images scene points both directly and after reflection by the mirror. As a result, scene points are imaged from different viewpoints within a single image.

The imaging system in this case captures the scene from the real viewpoint of the camera as well as a circular locus of virtual viewpoints produced by the mirror. To see this consider a radial slice of the imaging system that passes through the optical axis of the camera. The real viewpoint of the camera is located at O. The mirrors m1 and m2 (that are straight lines in a radial slice) produce the two virtual viewpoints V1 and V2, respectively, which are reflections of the real viewpoint O. Therefore, each radial slice of the system has two virtual viewpoints that are symmetric with respect to the optical axis. Since the complete imaging system includes a continuum of radial slices, it has a circular locus of virtual viewpoints whose center lies on the camera's optical axis.

The three viewpoints O, V1, and V2 in a radial slice project the scene onto a radial line in the image, which is the intersection of the image plane with that particular slice. This

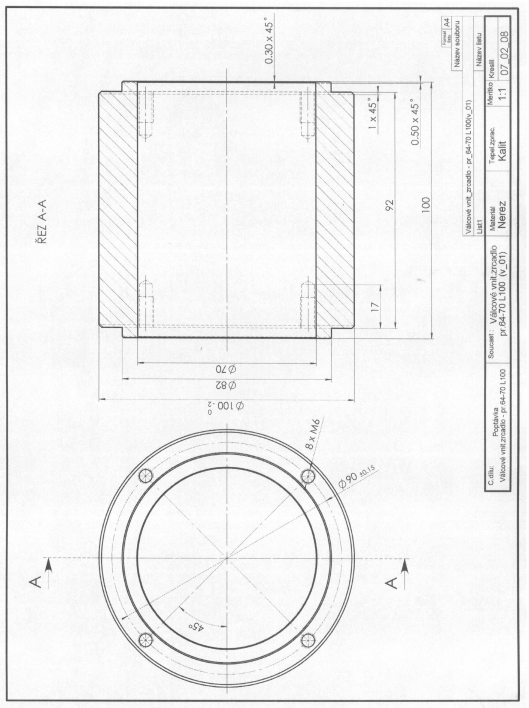

Figure 13: First design drawing of a cylindrical mirror.

radial image line has three segments - JK, KL, and LM. The real viewpoint O of the camera projects the scene onto the central part KL of the radial line, while the virtual viewpoints V1 and V2 project the scene onto JK and LM, respectively. The three viewpoints (real and virtual) capture only scene points that lie on that particular radial slice. If P is such a scene point, it is imaged thrice (if visible to all three viewpoints) along the corresponding radial image line at locations p, p1, and p2. Since this is true for every radial slice, the epipolar lines of such a system are radial. Since all radial image lines have three segments (JK, KL, and LM) and the lengths of these segments are independent of the chosen radial image line, the captured image has the form of a donut. The camera's real viewpoint captures the scene directly in the inner circle, while the annulus corresponds to reflection of the scene - the scene as seen from the circular locus of virtual viewpoints.

To determine the depth of a particular scene point, its projections in the image, i.e.,

corresponding points, have to be identified via stereo matching. As the epipolar lines are radial, the search for corresponding points needs to be restricted to a radial line in the image. However, most stereo matching techniques reported in literature deal with image pairs with horizontal epipolar lines. Therefore, it would be desirable to convert the information captured in the image into a form where the epipolar lines are horizontal. Recall that a radial line in the image has three parts - JK, KL, and LM, one for each viewpoint in the corresponding radial slice. We create a new image called the central view image by stacking the KL parts of successive radial lines. This view image corresponds to the central viewpoint in the radial slices. We create similar view images for the virtual viewpoints in the radial slices - the left view image by stacking the LM parts of successive radial lines and the right view image by stacking the JK parts. To account for the reflection of the scene by the mirror the contents of each JK and LM lines are flipped. Observe that the epipolar lines are now horizontal. Thus, traditional stereo matching algorithms can now be directly applied.

In the second case, the object is placed inside the cylindrical mirror, and the camera uses a fish-eye lens. In this case, the light rays are reflected more than once. We do not need to convert it into 3 or more images like what we did in the first case. Since in this case finding the angle of incidence can solve the depth problem without finding the image plane of each camera.

The conclusion is, the first approach is better than the second case. Hence, an MSS based on the first approach is being built now. The cylindrical mirror is currently being built by a company in central Europe (Czech Republic). The University has made the first payment. The second payment will be sent to that company when the mirror is delivered to our lab at the beginning of May. The Initial design the mirror is shown in Figure 13. An improved design is shown in Figure 14.

[Mesh Simplification] A mesh simplification technique by constricting triangles has been developed [113]. Constricting error is defined by a combination of squared volume error

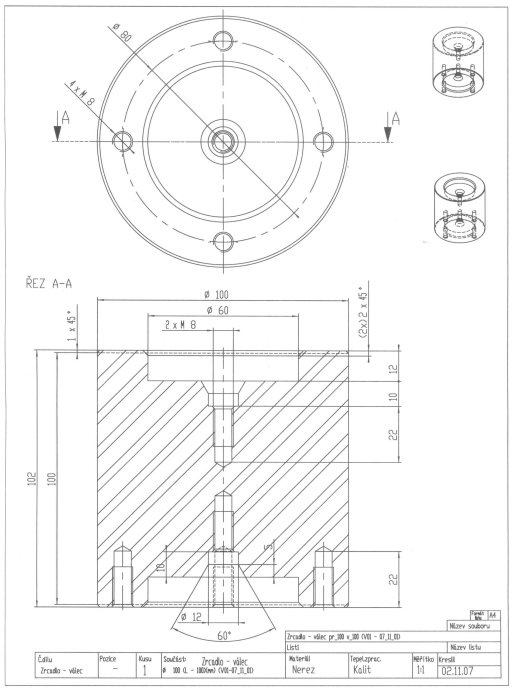

Figure 14: Second design drawing of a cylindrical mirror.

variation with constraint (SVEC), shape factor and normal constraint factor of triangles. Gaussian curvature factor of each constricted triangle is used to distinguish sharp feature triangles from blunter feature triangles. The triangle with the minimum constricting error is constricted first. New vertex locations of triangles with weaker feature are determined by minimizing the constriction error of the mesh model. For a sharp feature triangle, the vertex with maximal absolute Gaussian curvature of the three vertices is used as the new vertex. This new technique is simple, steady and can preserve mesh features well. An example of this technique is shown in Figure 17.

[**Construction of the gum model**] Our first attempt was performed at the Viz Center. The results were not acceptable (see Figures 15 and 15).

We then switch to a different appraoch. Instead of scanning gums we obtained from Dr. Burt, we scanned gums made of plaster (see Figure 16(a)). The result was quite good (see

(a) Gum model

(b) Scanned bottom gum

Figure 15: (a) Scanned gum model and (b) software processed scanned result.

Figure 16(b)).

(a) Plaster model

(b) Scanned result

Figure 16: (a) Plaster model used to build the gum model; (b) software processed result of the scanned upper gum.

The scanned results were then simplified using the result presented in [113]. The simplified results are shown in Figure 17).

The simplified meshes are then interpolated using our techniques to generate parametric representations (see Figure 18).

The parametrized representations are then extended to make the holes smaller so that

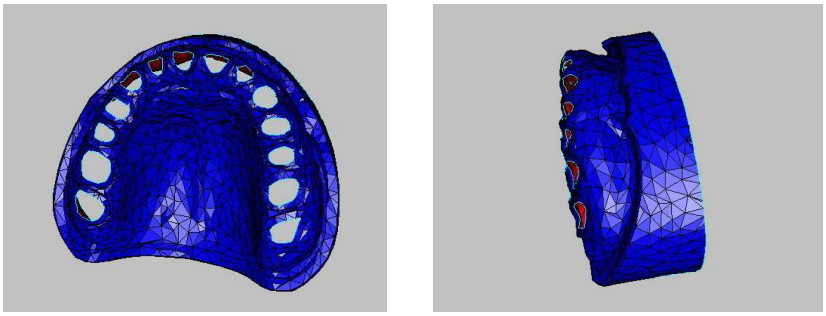

(a) Simplified gum I (b) Simplified gum II

Figure 17: Simplified gums.

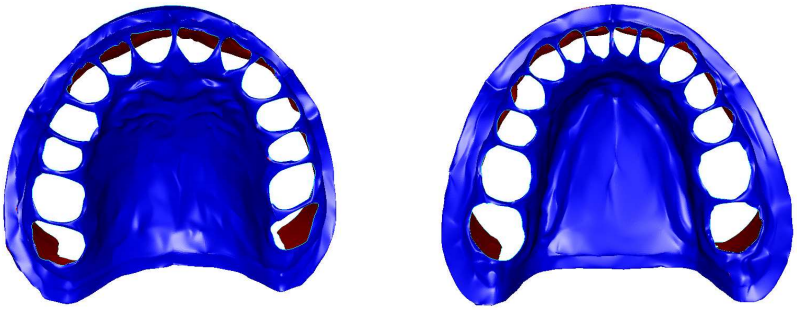

(a) Interpolated top gum (b) Interpolated bottom gum

Figure 18: Simplified gums are interpolated to create parametric representations.

when we put teeth into the holes, we will not get gaps anywhere in our model. The extended results are shown in Figure 19).

[**Standard Model**] With the extended gums and the simplified teeth, a standard model is then built by putting the teeth into the holes of the extended gums. Different views of the standard model are shown in Figure 20. We believe this is the best standard model we have seen so far.

[**Occlusion Model**] An occlusion model based on the standard model has been develope. Examples of the occlusion model are shown in Figure 21.

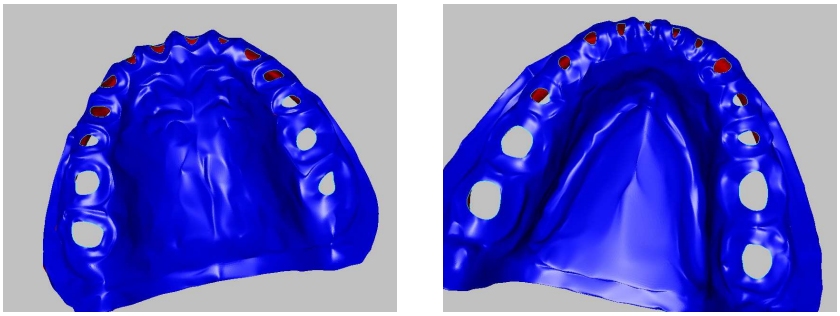

(a) extended top gum (b) Extended bottom gum

Figure 19: Extended gums.

[**Teeth and Gum Matching**] A curvature computing program has been built and tested during this time. With this program, features of a patient's teeth can be identified and compared with the standard model to identify the correspondence between the input teeth and teeth in our database. Teeth matching based on curvature distribution is currently been developed.

[**Teeth and Gum Segmentation**] A segmentation program has been developed. The teeth and the gums of the standard model are segmented using this technique and the results are shown in Figure 22. The original mesh is shown in Figure 20. Corrected We use different colors for different teeth and gums to show the correctness of our results.

[**Offset Surface Generation**] An offset surface generation technique for Loop subdivision surface has been developed.

[**Outcome Assessment**] We will use only one metric in assessing the outcome of the innovation research described above. We will consider the outcome a good one if the *relative error* in each case is smaller than or equal to 3% of the dimemsion of a tooth. Measuring *absolute error* does not make much sense here because the dimension of a tooth is already relatively small. The reason for using 3% for the relative error bound is because it corresponds to half a pixel in a resolution of 1280×960. This bound will be used both for DMR

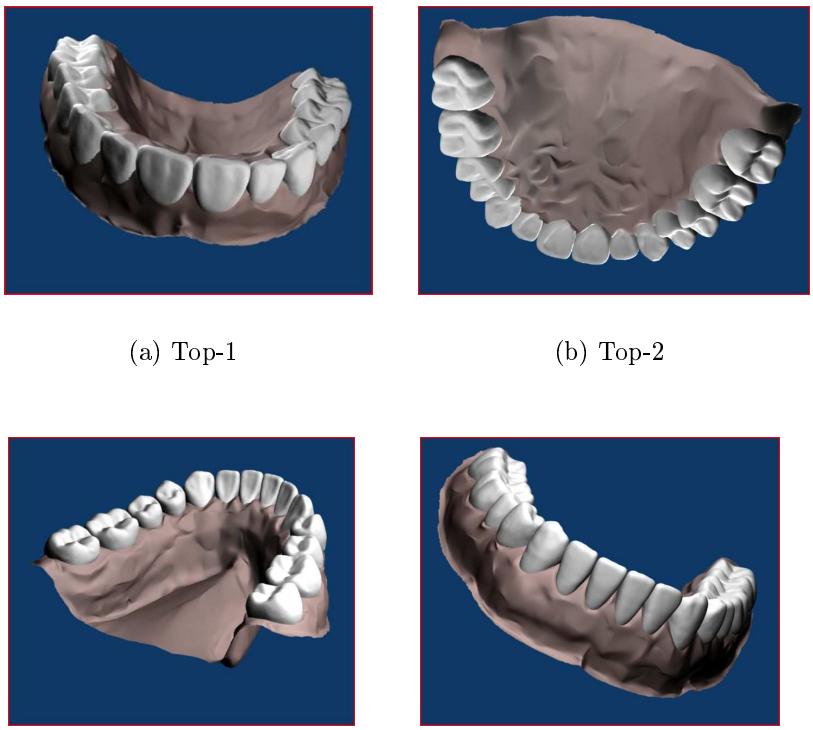

(a) Top-1 (b) Top-2

(c) Bottom-1 (d) Bottom-2

Figure 20: Standard model built by our team.

and shape representation.

6 Conclusions

Technical tasks finished during this 10-month period (6/1/07 - 3/31/08) include: the construction of a standard model, the construction of a occlusion model, the design of a mouth scan system, mesh simplification technique, mesh interpolation technique, mesh curvature computation technique, mesh segmentation technique, constraint based scaling, and offset surface generation technique. Technical tasks to be finished include: last step of the construction of the mouth scan system, and feature based matching technique.

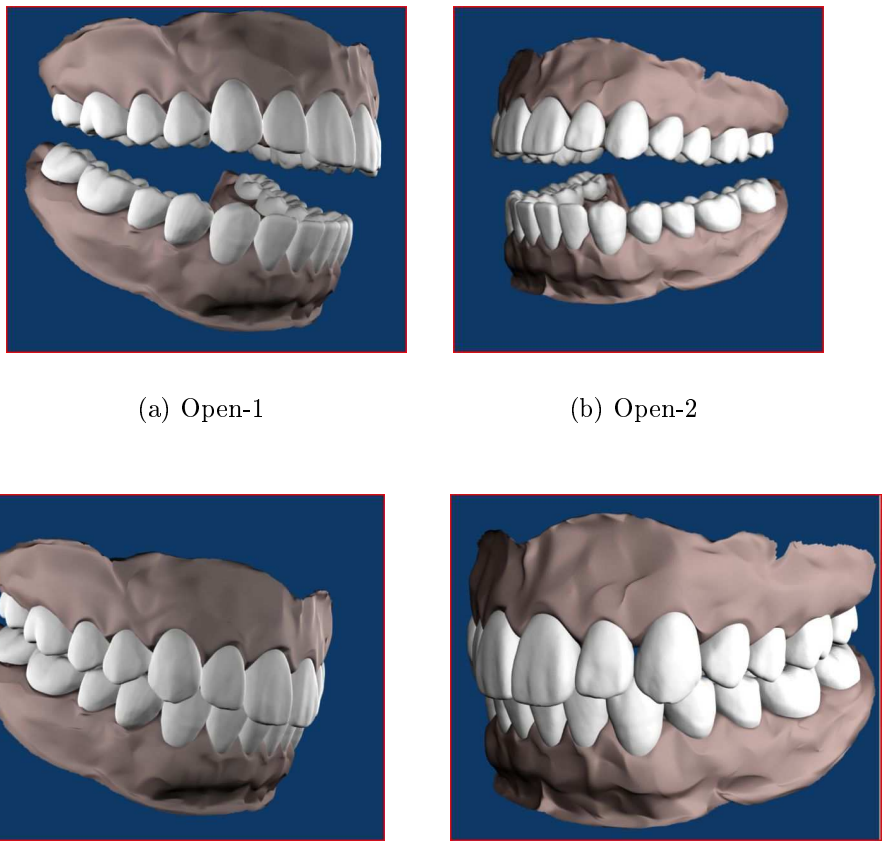

(a) Open-1 (b) Open-2

(c) Closed-1 (d) Closed-2

Figure 21: Occlusion model built by our team.

We consider this grant, up to this point, a success. We not only have reached most of our research goals, i.e., developing the necessary imaging system and required geometric algorithms to support the reproduction of a patient's mouth and occlusion, but also produced an MS (Ds. Jiaxi Wang, graduated in March, 2008, currently working for a company in Lexington, KY), 3 journal papers and 2 conference paper. We anticipate another MS (Mr. Conglin Huang) to be produced at the end of this year and a PhD (Mr. Fengtao Fan) to be produced at the end of next year.

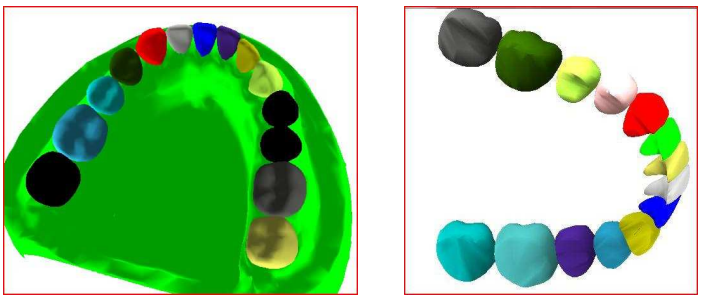

(a) Top-1 (b) Top-2

Figure 22: Results of segmenting the bottom teeth: (a) with gum; (b) without gum.

Acknowledgement

Research work presented in this report is supported by the Kentucky Science and Technology Corporation (grant number: KSTC-144-401-07-015). Teeth data and gum data used in this project are provided by Prof. H.T. Yao and his research group at the National Chung-Cheng University of Taiwan.

References

[1] Catmull E, Clark J. Recursively generated B-spline surfaces on arbitrary topological meshes, *Computer-Aided Design*, 1978, 10(6):350-355.

[2] D. Doo and M. A. Sabin. Behaviour of recursive subdivision surfaces near extraordinary points. *Computer-Aided Design*, 10:356-360, 1978.

[3] C.T. Loop, Smooth subdivision surfaces based on triangles, *M.S. Thesis*, Department of Mathematics, University of Utah, Salt Lake City, 1987.

[4] KOBBELT, L. $\sqrt{3}$ Subdivision, *Proceedings of SIGGRAPH 2000*, pp. 103-112, July, 2000.

[5] Ball AA, Storry DJT, Conditions for tangent plane continuity over recursively generated B-spline surfaces, *ACM Transactions on Graphics*, 1988, 7(2): 83-102.

[6] Ball AA, Storry DJT, An investigation of curvature variations over recursively generated B-spline surfaces, *ACM Transactions on Graphics*, 1990, 9(4):424-437.

[7] Biermann H, Kristjansson D, Zorin D, Approximate Boolean operations on free-form solids, *Proceedings of SIGGRAPH*, 2001: 185-194.

[8] Boier-Martin I, Zorin D, Differentiable Parameterization of Catmull-Clark Subdivision Surfaces, *Eurographics Symposium on Geometry Processing* (2004).

[9] Chen G, Cheng F, Matrix based Subdivision Depth Computation Method for Extra-Ordinary Catmull-Clark Subdivision Surface Patches, *Lecture Notes in Computer Science*, Vol. 4077, Springer, 2006, 545-552.

[10] Cheng F, Yong J, Subdivision Depth Computation for Catmull-Clark Subdivision Surfaces, *Computer Aided Design & Applications 3*, 1-4, 2006.

[11] Cheng F, Chen G, Yong J, Subdivision Depth Computation for Extra-Ordinary Catmull-Clark Subdivision Surface Patches, *Lecture Notes in Computer Science*, Vol. 4035, Springer, 2006, 545-552.

[12] DeRose T, Kass M, Truong T, Subdivision Surfaces in Character Animation, *Proc. of SIGGRAPH*, 1998.

[13] Halstead M, Kass M, DeRose T, Efficient, fair interpolation using Catmull-Clark surfaces, *Proceedings of SIGGRAPH*, 1993:35-44.

[14] Litke N, Levin A, Schröder P, Trimming for Subdivision Surfaces, *Computer Aided Geometric Design* 2001, 18(5):463-481.

[15] Reif U, A unified approach to subdivision algorithms near extraordinary vertices, *Computer Aided Geometric Design*, 1995, 12(2): 153-174.

[16] Jörg Peters, Ulrich Reif , Analysis of Algorithms Generalizing B-Spline Subdivision, *SIAM Journal of Numerical Analysis*, Vol. 35, No. 2, pp. 728-748, 1998.

[17] Lutterkort D, Peters J, Tight linear envelopes for splines, *Numerische Mathematik 89*, 4, 735-748, 2001.

[18] Peters J, Patching Catmull-Clark Meshes, *Proceedings of SIGGRAPH 2000*, 255-258.

[19] Sederberg TW, Zheng J, Sewell D, Sabin M, Non-uniform recursive subdivision surfaces, *Proceedings of SIGGRAPH*, 1998:19-24.

[20] Stam J, Exact Evaluation of Catmull-Clark Subdivision Surfaces at Arbitrary Parameter Values, *Proceedings of SIGGRAPH* 1998:395-404.

[21] Stam J, Evaluation of Loop Subdivision Surfaces, *SIGGRAPH'99 Course Notes*, 1999.

[22] Peter Schröder, Denis Zorin, Subdivision for Modeling and Animation, *SIGGRAPH'98 Course Notes*, 1998.

[23] Zorin, D., Schröder, P., and Sweldens, W. Interactive Multiresolution Mesh Editing. In *Proceedings of SIGGRAPH 1997*, 259-268.

[24] Joe Warren, Henrik Weimer, Subdivision Methods for Geometric Design: A Constructive Approach. ISBN: 1-55860-446-4, Academic Press, 2002.

[25] Kobbelt, L., Interpolatory subdivision on open quadrilateral nets with arbitrary topology, *Computer Graphics Forum*, Eurographics, V.15, 1996.

[26] D. Zorin, P. Schröder, W. Sweldens, Interpolating Subdivision for meshes with arbitrary topology, *ACM SIGGRAPH*, 1996:189-192.

[27] Dyn,N., Levin, D., and Gregory, J. A., A butterfly subdivision scheme for surface interpolation with tension control, *ACM Transactions on Graphics*, 9, 2 (1990) 160-169.

[28] Nasri, A. H., Surface interpolation on irregular networks with normal conditions, *Computer Aided Geometric Design*, 8 (1991), 89-96.

[29] Garland M, Heckber P, Surface simplification using quadric error metrics, *Proceedings of SIGGRAPH* 1997:209-216.

[30] Settgast V, Müller K, Fünfzig C, et.al., Adaptive Tesselation of Subdivision Surfaces, In *Computers & Graphics*, 2004, pp:73-78.

[31] Amresh A, Farin G, Razdan A, Adaptive Subdivision Schemes for Triangular Meshes, In *Hierarchical and Geometric Methods in Scientific Visualization*, Springer-Verlag, 2002 pp:319-327.

[32] Wu X, Peters J, An Accurate Error Measure for Adaptive Subdivision Surfaces, In *Shape Modeling International*, 2005

[33] M. Böo, M. Amor, M. Doggett, et.al., Hardware Support for Adaptive Subdivision Surface Rendering, In *Proceedings of the ACM SIGGRAPH/EUROGRAPHICS workshop on Graphics hardware* 2001, pp:33-40.

[34] Isenberg T, Hartmann K, König H, Interest Value Driven Adaptive Subdivision, In *Simulation und Visualisierung*, March 6-7, 2003, Magdeburg, Germany.

[35] Sovakar A, Kobbelt L, API Design for adaptive subdivision schemes. 67-72, *Computers & Graphics*, Vol. 28, No. 1, Feb. 2004.

[36] Rose D, Kada M, Ertl T, On-the-Fly Adaptive Subdivision Terrain. In *Proceedings of the Vision Modeling and Visualization Conference*, Stuttgart, Germany, pp: 87-92, Nov. 2001.

[37] Yong J, Cheng F, Adaptive Subdivision of Catmull-Clark Subdivision Surfaces, *Computer-Aided Design & Applications* 2(1-4):253-261, 2005.

[38] Kersey S N, Smoothing and near-interpolatory subdivision surfaces, www.cs.georgiasouthern.edu/faculty/kersey_s/ private/res/siam2003.pdf

[39] Levin A, Interpolating nets of curves by smooth subdivision surfaces, *ACM SIGGRAPH*, 1999, 57-64.

[40] Litke N, Levin A, Schröder P, Fitting subdivision surfaces, *Proceedings of the conference on Visualization* 2001:319-324.

[41] Nasri A H, Sabin M A, Taxonomy of interpolation constraints on recursive subdivision curves, *The Visual Computer*, 2002, 18(4):259-272.

[42] Schaefer S, Warren J, A Factored Interpolatory Subdivision Scheme for Quadrilateral Surfaces, *Curves and Surface Fitting*, 2002, 373-382.

[43] Peters J, C1-surface splines. *SIAM Journal on Numerical Analysis* 1995, 32(2):645-666.

[44] Schaefer S., Warren, J., Zorin, D., Lofting curve networks using subdivision surfaces, *Proc 2004 Eurographics symposium on Geometry processing*, 2004:103-114.

[45] Baker, T. J., Interpolation from a cloud of points, *Proceedings, 12th International Meshing Roundtable*, Sandia National Laboratories, pp.55-63, Sept 2003.

[46] Xunnian Yang, Surface interpolation of meshes by geometric subdivision, *Computer-Aided Design*, 2005, 37(5):497-508.

[47] Kestutis Karciauskas and Jörg Peters, Guided Subdivision, http://www.cise.ufl.edu/research/ SurfLab/papers/05guiSub.pdf, 2005.

[48] Shuhua Lai, Fuhua (Frank) Cheng, Similarity based Interpolation Using Catmull-Clark Subdivision Surfaces, *The Visual Computer* 22,9-11 (October 2006), 865-873.

[49] Shuhua Lai, Fuhua (Frank) Cheng, Inscribed Approximation based Adaptive Tessellation, *International Journal of CAD/CAM*, Vol. 6, No. 1, 2006.

[50] Shuhua Lai, Fuhua (Frank) Cheng, Voxelization of Free-form Solids Represented by Catmull-Clark Subdivision Surfaces, *Lecture Notes in Computer Science*, Vol. 4077, Springer, 2006, pp. 595-601.

[51] Shuhua Lai, Fuhua (Frank) Cheng, Parametrization of Catmull-Clark Subdivision Surfaces and its Applications, *Computer Aided Design & Applications*, 3, 1-4, 2006.

[52] Shuhua Lai, Fuhua (Frank) Cheng, Near-Optimum Adaptive Tessellation of General Catmull-Clark Subdivision Surfaces, *CGI 2006*, *Lecture Notes in Computer Science*, Vol. 4035, Springer, 2006, pp. 562-569.

[53] Shuhua Lai, Fuhua (Frank) Cheng, Texture Mapping on Surfaces of Arbitrary Topology using Norm Preserving based Optimization, *The Visual Computer*, 21(1-8):783-790, 2005.

[54] Shuhua Lai, Fuhua (Frank) Cheng, Adaptive Rendering of Catmull-Clark Subdivision Surfaces, *9th International Conference of Computer Aided Design & Computer Graphics*, 125-130, 2005.

[55] Shuhua Lai, Shiping Zou, Fuhua (Frank) Cheng, Constrained Scaling of Catmull-Clark Subdivision Surfaces, *Computer Aided Design & Applications*, 1(1-4): 7-16, 2004.

[56] Shuhua Lai, Fuhua (Frank) Cheng, Robust and Error Controllable Boolean Operations on Free-Form Solids Represented by Catmull-Clark Subdivision Surfaces, Submitted.

[57] V. Settgast, K. Müler, Christoph Füfzig et.al., Adaptive Tesselation of Subdivision Surfaces in OpenSG, In *Proceedings of OpenSG Symposium*, 2003, pp:39-47.

[58] Matthias Zwicker, Hanspeter Pfister, Jeroen van Baar, Markus Gross, Surface Splatting, *SIGGRAPH 2001.*

[59] D. Gonsor and M. Neamtu. Subdivision surfaces - can they be useful for geometric modeling applications?, *Technical Report, Boeing Technical Report 01-011*, Boeing Company, 2001.

[60] Wang H, Qin K, 2004. Estimating Subidivision Depth of Catmull-Clark Surfaces. *J. Comput. Sci. & Technol. 19*, 5, 657-664.

[61] Wu X, Peters J, An Accurate Error Measure for Adaptive Subdivision Surfaces, *Proc. Shape Modeling International 2005*, 1-6.

[62] AFT Digital, Roswell, GA, USA (http://www.lightyeardirect.com/)

[63] Ambrosio L, Montegazza C, Curvature and distance function from a manifold, *J. Geomet. Analy.* 1998, 8:723-748.

[64] Amenta N, Marshall B, Manolis K, A New Voronoi-Based Surface Reconstruction Algorithm, *Computer Graphics* (proc. of SIGGRAPH '98) 1998, 415-421.

[65] Austin SP, Jerard RB, Drysdale RL, Comparison of discretization algorithms for NURBS surfaces with application to numerically controlled machining, *Computer Aided Design* 1997, 29(1): 71-83.

[66] Bajaj C, Bernardini F, Xu G, Automatic Reconstruction of Surfaces and Scalar Fields from 3D Scans, *Computer Graphics* (proc. of SIGGRAPH '95) 1995, 109-118.

[67] Barnhill R, Frost TM, Parametric Offset Surface Approximation, *Computing Supplement* 1995, 10:1-34.

[68] BEGO Medical AG, Bremen, Germany (www.bego-medical.de/)

[69] Belongie S, Malik J, Puzicha J, Matching Shapes, *proc Int. Conf. Computer Vision 2001*

[70] Belongie S, Malik J, Puzicha J, Shape Matching and Object Recognition Using Shape Contexts, *IEEE Transactions on Pattern Analysis and Machine Intelligence* 2002, 24(4):509-522.

[71] Berg AC, Berg TL, Malik J, Shape Matching and Object Recognition using Low Distortion Correspondence, *proc of IEEE Computer Vision and Pattern Recognition 2005*

[72] Besl PJ, Jain RC, Segmentation through Variable-order Surface Fitting, *IEEE Transactions on Pattern Analysis and Machine Intelligence* 1988, 10(2):167-192.

[73] Bien A, Cheng F, A Blending Model for Parametrically Defined Geometric Objects, *Proc. ACM Solid Modeling'91 Conference* 1991, 339-347.

[74] Brontes Technologies, Lexington, MA, USA (www.brontes3d.com/)

[75] Cad.esthetics AB, Skelleftea, Sweden (www.cadesthetics.com/)

[76] Catmull E, Clark J, Recursively generated B-spline surfaces on arbitrary topological meshes, *Computer-Aided Design*, 1978, 10(6):350-355.

[77] Canny J, A Computational Approach to Edge Detection, *IEEE Transactions on Pattern Analysis and Machine Intelligence* 1986, 8(6):679-698.

[78] Cheng D, Wang W, Qin H, Wong KK, Yang H, Liu Y, Fitting subdivision surfaces to unorganized point data using SDM, *Proc 12th Pacific Graphics*, IEEE Computer Society Press, 2004, 16-24.

[79] Cohen J, Olano M, Manocha D, Appearance-Preserving Simplification, *Computer Graphics* (Proc. of SIGGRAPH 98), 1998, 115-122.

[80] Cynovad, Saint-Laurent, Quebec, Canada (www.cynovad.com/)

[81] Dalmia AK, Trivedi MM, Acquisition of 3D structure of selectable quality from image streams, *IEEE Workshop on Applications of Computer Vision*, 1994, 289-296.

[82] Davis J, Yang R, Wang L, BRDF invariant stereo using light transport constancy, *Proc. International Conference on Computer Vision (ICCV)*, 2005, 436-443.

[83] DCS AG, Allschwil, Switzerland (www.dcs-dental.com/)

[84] Degudent, Frankfurt, Germany (www.degudent.de/)

[85] DePiero F, Trivedi MM, 3-D Computer Vision using Structured Light: Design, Calibration, and Implementation Issues *Advances in Computers*, 2006, 43:243-278.

[86] Dhond U, Aggrawal J, Structure from Stereo: a Review, *IEEE Transactions on Systems, Man, and Cybernetics*, 1989, 19(6):1489-1510.

[87] Hint-ELs, Griesheim, Germany (www.hintel.de/)

[88] etkon AG, Grafelfingen, Germany (www.etkon.de/)

[89] Fang L, Gossard D, Reconstruction of Smooth Parametric Surfaces from Unorganized Data Points, *Curves and Surfaces in Computer Vision and Graphics* 1992, Vol. 1830, SPIE, 226-236.

[90] Farin G, *Curves and Surfaces for Computer Aided Geometric Design*, Academic Press, San Diego, 1990.

[91] Piegl L, Tiller W, *The NURBS Book*, 2nd edition, Springer-Verlag, New York, 1997.

[92] Fasbinder DJ, Clinical Performance of Chairside CAD/CAM Restorations, *Journal of American Dental Association* 2006, 137(Special supplement):22s-31s.

[93] Forster F, A High-Sesolution and High Accuracy Real-Time 3D Sensor based on Structured Light, *Proc. 3rd Int. Sym. on 3D Data Processing, Visulization, and transmission (3DPVT'06)*, 2006, 208-215.

[94] Frigerio F, Hart DP, Calibrationless Aberration Correction through Active Wavefront Sampling (AWS) and Multi-Camera Imaging, *Proc. 13th Int. Symp on Appl. Laser Techniques to Fluid Mechanics* 2006.

[95] Gendex Dental Systems, Lake Zurich, IL, USA (http://www.gendex.com/)

[96] Giordano R, CAD/CAM: an overview of machines and materials, *J Dent Technol* 2003, 20:20-30.

[97] GC international, Tokyo, Japan (www.gcdental.co.jp/cadcam/index.html)

[98] Goshtasby A, Nambala S, deRijk WG, Campbell SD, A System for Digital Reconstruction of Gypsum Dental Casts, *IEEE Trans. Medical Imaging* 1997, 16(5):664-674.

[99] Gluckman J, Nayar SK, Planar Catadioptric Stereo: Geometry and Calibration, *Proc. Computer Vision and Pattern Recognition (CVPR)*, 1999, 1022-1028.

[100] Guo B, Menon J, Willette B, Surface Reconstruction Using Alpha Shapes, *Computer Graphics Forum* 1997, 16(4):177-190.

[101] Hoppe H, DeRose T, Duchamp T, McDonald J, Stuetzle W, Surface Reconstruction from Unorganized Points, *Computer Graphics* (proc. of SIGGRAPH '92) 1992, 71-78.

[102] Hoppe H, DeRose T, Duchamp T, McDonald J, Stuetzle W, Mesh Optimization, *Computer Graphics* (proc. of SIGGRAPH '93) 1993, 19-26.

[103] Hoppe H, DeRose T, Duchamp T, Halstead M, Jin H, McDonald J, Schweitzer J, Stuetzle W, Piecewise smooth surface reconstruction, *Computer Graphics* (proc. of SIGGRAPH '94) 1994, 295-302.

[104] Hoppe H, Progressive Meshes, *Computer Graphics* (proc. of SIGGRAPH '96) 1996, 99-108.

[105] Huang M, Wang R, Thompson V, Rekow D, Soboyejo WO, Bioinspired design of dental multilayers. *J Mater Sci Mater Med.* 2007, 18(1):57-64.

[106] Kavo, Leutkirch, Germany (www.kavo-everest.com/)

[107] Khodakovsky A, Schroder P, Sweldens W, Progressive Geometry compression, *proc. of SIGGRAPH 2000* 271-278.

[108] Khodakovsky A, Guskov l, Normal mesh compression, in *Geometric Modeling for Scientific Visualization* 2004, 189-206.

[109] Kodak Dental System, USA (http://www.kodakdental.com/)

[110] Krishnamurthy V, Levoy M, Fitting Smooth Surfaces to Dense Polygon Meshes, *Computer Graphics* (proc. of SIGGRAPH '96) 1996, 303-312.

[111] Lin S-S, Bajcsy R, High Resolution Catadioptric Omni-Directional Stereo Sensor for Robot Vision, *Proc. ICRA*, 2003, 1694–1699.

[112] Liu L, Zhang C, Cheng F, Parametrization of Quadrilateral Meshes, *Lecture Notes in Computer Science*, Vol. 4488 (2007), Springer, 17-24.

[113] Zhou Y, Zhang C, Cheng F, Mesh Simplification by Volume Variation with Feature Preserving, *in preparation.*

[114] Laurendeau D, Guimond L, Poussart D, A Computer-Vision Technique for the Aquisition and Processing of 3-D Profiles of Dental Imprints: An Application in Orthodontics, *IEEE Transactions on Medical Imaging* 1991, 10(3):453-461.

[115] Lee NL, Feature Recognition from Scanned Data Points, *PhD Thesis, The Ohio State University,* 1995.

[116] Level D, Sharir M, An Efficient and Simple Motion Planning Algorithm for a Ladder Amidst Polygonal Barriers, *Journal of Algorithms* 1987, 8:192-215.

[117] Lozano-Perez T, Wesley MA, An Algorithm for Planning Collision-Free Paths Among Polyhedral Obstracles, *Communications of the ACM* 1979, 22:560-570.

[118] Moore M, Wilhelms J, Collision Detection and Response for Computer Animation, *Computer Graphics* (proc. of SIGGRAPH '88) 1988, 22:289-298.

[119] Mori G, Belongie S, Malik J, Shape Contexts Enable Efficient Retrieval of Similar Shapes, *proc of IEEE Computer Vision and Pattern Recognition 2001*

[120] Mörmann WH, Lutz F, Gotsch T, CAD-CAM ceramic inlays and onlays: a case report after 3 years in place, *Journal of the American Dental Association* 1990, 120:517-520.

[121] Mörmann WH, The origin of the CEREC method: a personal review of the first 5 years, *Int J Comput Dent* 2004, 7(1):11-24.

[122] Mörmann WH, Brandestini M, The fundamental inventive principles of CEREC CAD/CAM, in *Mörmann WH, ed. State of the art of CAD/CAM restorations: 20 years of CEREC*, London:Quintessence; 2006:1-8.

[123] Mörmann WH, The evolution of the CEREC system, *Journal of American Dental Association* 2006, 137(Special supplement):7s-13s.

[124] Nakamura T, Hirata T, Maruyama T, Computer Technology on Esthetic Dentistry - Dental CAD/CAM and Computer Imaging System, *Esthetic Dentistry* 1993, 5(1):1-6.

[125] Mayar SK, Sphereo: Recovering depth using a single camera and two specular spheres, *Proceedings of SPIE: Optzcs, Illumination, and Image Sensing for Machine Vision 11*, 1988.

[126] Mayar SK, Baker S, Catadioptric Image Formation, *Proc. DARPA Image Understanding Workshop*, 1997.

[127] Kuthirummal S, Nayar SK, Multiview Radial Catadioptric Imaging for Scene Capture, *ACM Trans. on Graphics* (also Proc. of ACM SIGGRAPH), 2006.

[128] Nayar SK, Krishnan G, Grossberg MD, Raskar R, Fast Separation of Direct and Global Components of a Scene using High Frequency Illumination, *ACM Trans. on Graphics* (also Proc. of ACM SIGGRAPH), 2006.

[129] Nene S, Mayar SK, Stereo with Mirrors, *Proc. 6th International Conference on Computer Vision*, 1998, 1087-1094.

[130] O'Brien N, Jain R, Axial motion stereo, *Proc. IEEE Workshop Computer Vision*, 1984, 88-92.

[131] Pottmann H, Leopoldseder S, Hofer M, Approximation with active b-spline curves and surfaces, *Proc 10th Pacific Graphics*, IEEE Computer Society press, 2002, 8-25.

[132] Pottmann H, Hofer M, Geometry of the squared distance function to curves and surfaces, in *Visualization and Mathematics III*, H. Hege and K. Polthier, Eds., 2003, 223-244.

[133] Nobel Biocare, Goteburg, Sweden (www.nobelbiocare.com/)

[134] Sederberg TW, Zheng J, Sewell D, Sabin M, Non-uniform recursive subdivision surfaces, *Proceedings of SIGGRAPH*, 1998:19-24.

[135] Shen TS, Huang J, Menq CH, Multiple-Sensor Integration for Rapid and High-Precision Coordinate metrology, *IEEE/ASME Transactions on Mechatronics* 2006, 5(2):110-121.

[136] Sirona Dental Systems, Bensheim, Germany (http://www.sirona.com/)

[137] Southwell D, Basu A, Fiala M, Reyda J, Panoramic Stereo, *Proc. International Confeyence on Pattern Recognition (ICPR)*, 1996:378-382.

[138] Strub JR, Rekow ED, Witkowski S, Computer-aided design and fabrication of dental restorations: Surrent systems and future possibilities, *Journal of American Dental Association* 2006, 137(9):1289-1296.

[139] Su W, Axial Motion Stereo Vision and Structured Light for 3D Acquisition of the Human Ear, *PhD Thesis*, ECE Dept, University of Kentucky, 2006.

[140] Suni Medical Imaging, San Jose, CA, USA (http://www.suni.com/)

[141] Tanaka F, Kishinami T, Computer Model of Teeth Row and Occlusion Movement Simulation, *4th Sapporo International Computer Graphics Symposium* 1990.

[142] Technologyinsider (www.epoch.org.tw/upload/startup.2005.ILP.pdf)

[143] 3M ESPE, Seefeld, Germany (http://cms.3m.com/cms/US/en/2-2/kzikuFW/view.jhtml)

[144] Tinschert J, Natt G, Hassenpflug S, Spiekermann H, Status of current CAD/CAM technology in dental medicine, Surrent systems and future possibilities, *Int J Comput Dent* 2004, 7(1):25-45.

[145] TurboDent System, Taichung, Taiwan (http://www.taiwandent.com/)

[146] Tsai RY, A Versatile Camera Calibration Technique for High-Accuracy 3D Machine Vision Metrology Using Off-the-Shelf TV Cameras and Lenses, *IEEE Journal of Robotics and Automation*, 1987, RA-3(4):323-344.

[147] Uranishi Y, Three-Dimensional Measurement System Using a Cylindrical Mirror, *Master's Thesis*, Department of Information Processing, Graduate School of Information Science, Nara Institute and Technilogy, Japan, 2005.

[148] Varady T, Martin RR, Cox J, Reverse Engineering of Geometric Modeling - an Introduction, *Computer-Aided Design*, 1997, 29(4):255-268.

[149] Wang W, Pottmann H, Liu Y, Fitting B-spline curves to point clouds by curvature-based squared distance minimization, *ACM Transactions on Graphics*, 2006, 25(2):214-238.

[150] Whitaker R, Breen D, Museth K, Soni N, Segmentation of biological datasets using a level-set framework, in *M Chen and A. Kaufman, Editors, Volume Graphics* 2001, Springer, Vienna, 249-263.

[151] Wieland Dental + Technik GmbH, Pforzheim, Germany (www.wielang-dental.de/)

[152] Witkowski S, (CAD-)/CAM in dental technology, *Quintessence Dent Technol* 2005, 28:169-184.

[153] Wol-Dent, Ludwigshafen, Germany (www.wolzdental.com/)

[154] Zheng J, Cai Y, Making Doo-Sabin surface interpolation always work over irregular meshes, *The Visualization Computer*, 2005, 21:242-251.

[155] Yang R, Pollefeys M, Multi-Resolution Real-Time Stereo on Commodity Graphics Hardware, *Proc. Computer Vision and Pattern Recognition (CVPR)*, 2003, 211-218.

[156] Yang Z, Wang YF, Error ananysis of 3D shape construction from structured lighting, *Pattern Recognition*, 1996, 23(2):189-206.

[157] Zhang S, Huang P, High-resolution, Real-time 3D Shape Acquisition, *Proc. 2004 IEEE Computer Society Conference on Computer Vision and Pattern Recognition Workshops (CVPRW'04)*, 2004, 1063-1069.

[158] Zheng J, Cai Y, Interpolation over Arbitrary Topology Meshes Using a Two-Phase Subdivision Scheme, *IEEE Transactions on Visualization and Computer Graphics*, 2006, 12(3):301-310.

[159] Zorin D, Kristjansson D, Evaluation Piecewise Smooth Subdivision Surfaces, *The Visual Computer* 2002, 18(5/6):299-315.